Results in Engineering 27 (2025) 106502

Contents lists available at ScienceDirect

Results in Engineering

journal homepage: www.sciencedirect.com/journal/results-in-engineering

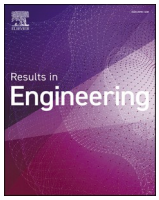

Research paper

Economic and performance optimization of hollow fiber forward osmosis using treated sewage effluent and novel sodium metasilicate sol-gel draw solution

Firas Alkadour [a], Kenan A. Alkhamri [a], Tayma Kazwini [b], Ali Altaee [b], Maryam AL-Ejji [c], Probir Das [d], Alaa H. Hawari [a,*]

[a] Department of Civil and Environmental Engineering, College of Engineering, Qatar University, PO Box 2713, Doha, Qatar
[b] School of Civil and Environmental Engineering, University of Technology Sydney, 15 Broadway, Ultimo, NSW 2007, Australia
[c] Center for Advanced Materials, Qatar University, PO Box 2713, Doha, Qatar
[d] Algal Technologies Program, Center for Sustainable Development, College of Arts and Sciences, Qatar University, 2713, Doha, Qatar

ARTICLE INFO

Keywords:
Forward osmosis
Hollow fiber
Sol-gel draw solution
Economic feasibility
Operational parameters

ABSTRACT

This study integrates performance optimization with an economic analysis of a hollow fiber forward osmosis (HFFO) system using a novel sodium metasilicate (SMS)-based sol-gel draw solution. The SMS sol-gel is diluted during the FO process using treated sewage effluent as the feed solution, addressing wastewater reuse challenges. Unlike conventional draw solutions requiring energy-intensive regeneration, the diluted SMS is directly applied for soil enhancement, eliminating regeneration needs. Optimized parameters include feed flow rates (60–80 L/h), draw flow rates (50–75 L/h), transmembrane pressure (0.2–0.3 bar), and a draw solution molarity of 0.3 M. The system achieved a peak water flux of 17.82 LMH in AL-DS orientation and an ion rejection rate of 97.8 %. Notably, the specific solution cost (SSC) varied between $0.16 and $0.37 per cubic meter, depending on operational parameters, with the optimized system achieving the lowest SSC of $0.16 per cubic meter, demonstrating significant cost-effectiveness and sustainability.

1. Introduction

Sodium metasilicate (SMS) has emerged as a significant agent in soil treatment and stabilization, particularly noted for its ability to enhance soil strength and durability when used in conjunction with other stabilizers [1]. Upon dissolution, SMS generates a colorless alkaline solution rich in silicon, which provides numerous agronomic benefits. These benefits include improved soil quality, enhanced nutrient availability, better water retention, increased resistance to plant diseases, and greater tolerance to environmental stressors [2,3]. Empirical studies have corroborated the positive impact of SMS on plant growth; for instance, Mali and Aery (2008) reported enhanced germination and growth of wheat [4], while Zhou et al. [5] observed improved growth and pathogen resistance in cucumbers [5].

Despite the advantages offered by SMS, its preparation necessitates freshwater, a resource often scarce in arid regions. To mitigate this challenge, innovative membrane technologies, such as forward osmosis (FO), can be employed for desalination and wastewater treatment, thereby ensuring a reliable supply of freshwater, as well as its role in the circular economy through nutrient extraction such as phosphate [6]. Unlike traditional pressure-driven processes, FO leverages osmotic pressure differentials across a semi-permeable membrane, facilitating the natural migration of water from a less concentrated feed solution to a more concentrated draw solution [7–9]. The FO process presents several benefits, including lower energy requirements, reduced membrane fouling, and decreased operational costs [10–12]. A consistent rise in FO research over the past decade reflects this growing interest; however, limited large-scale implementation and economic uncertainties remain key barriers [13]. One of the major cost-related challenges lies in the energy demands associated with draw solution regeneration. For instance, a study by Junco et al. outlines a scenario where the use of a less efficient osmotic agent resulted in regeneration energy costs that outweighed the anticipated savings from the FO process [14].

Recent research by Kazwini et al. [15] explored the use of flat sheet membranes (FSM) in FO applications with SMS-based sol-gel as a draw solution and seawater as the feed solution. The SMS-based sol-gel draw

* Corresponding author at: Department of Civil and Environmental Engineering, College of Engineering, Qatar University, 2713 Doha, Qatar.
E-mail address: a.hawari@qu.edu.qa (A.H. Hawari).

https://doi.org/10.1016/j.rineng.2025.106502
Received 17 May 2025; Received in revised form 13 July 2025; Accepted 27 July 2025
Available online 28 July 2025

solution was prepared through the reaction of SMS with nitric acid, yielding silicic acid and sodium nitrate. Their findings demonstrated the potential of this approach to enhance soil water retention and nutrient supply [15]. However, the study lacked comprehensive performance optimization and economic evaluation, which are essential to fully realize the potential of SMS-based FO systems.

The selection of membranes plays a crucial role in the efficiency of FO systems, as material composition, structure, and fabrication method directly influence their performance [16]. Hollow fiber forward osmosis (HFFO) membranes are particularly suited for FO applications due to their high surface area-to-volume ratio, which enhances mass transfer efficiency and enables compact system designs [17]. They also offer excellent mechanical stability and low resistance to solute diffusion, maximizing osmotic pressure and improving water flux (Jw) [18,19]. Among them, Aquaporin-based HFFO membranes, further enhance performance by incorporating transmembrane proteins that facilitate rapid water transport while maintaining high selectivity and low reverse solute flux (RSF) [20,21]. Previous studies on HFFO membranes, including those conducted by Jalab et al. [22], Sanahuja-Embuena et al. [17], Shibuya et al. [23] and Li et al. [24], have primarily focused on effects of operational parameters on performance metrics. However, these studies have largely overlooked the critical aspect of economic feasibility.

To address these gaps, this paper presents a novel approach that integrates both performance and economic optimization of HFFO system using a newly applied SMS-based sol-gel draw solution in combination with treated sewage effluent (TSE) as the feed. The draw solution is progressively diluted through the FO process for direct soil application, thereby eliminating the need for regeneration. Key operational parameters—feed and draw flow rates, transmembrane pressure (TMP), solute concentration, and membrane orientation—are analyzed for their effects on system performance, including water flux, reverse solute flux, and specific reverse solute flux (SRSF), as well as overall system cost.

2. Materials and setup

2.1. Membrane characterization

Optimal forward osmosis (FO) membranes feature an ultra-thin, dense selective layer to ensure high water permeability and solute rejection, supported by a thin, porous layer for mechanical stability and minimal resistance to solute diffusion. This design maximizes osmotic pressure while mitigating internal concentration polarization (ICP) and external concentration polarization (ECP), which can hinder mass transfer [25,26]. Additionally, high membrane hydrophilicity also helps in fouling reduction [27]. In this study, Aquaporin-based HFFO membrane was utilized, which features aquaporins—transmembrane proteins that enable rapid water transport [20,21]. Compared to conventional polymeric membranes, Aquaporin-based membranes offer superior water permeability and selectivity while maintaining high Jw with minimal RSF [20,21]. The Aquaporin-based HFFO membrane used in this study incorporates a TFC structure, similar to recent TFC-FO membranes enhanced with hydrophilic interlayers to improve selectivity and flux [28]. Detailed specifications of the Aquaporin membrane module used in this study are summarized in Table 1.

2.2. Feed solution and draw solution preparation

The feed solution (FS) used in the FO process was TSE obtained from a Doha wastewater facility. It had a total dissolved solids (TDS) concentration of 2816 mg/L, along with minor amounts of phosphorus, nitrogen, and organic materials, making it unsuitable for direct application in irrigation. To simulate the TSE, the FS was prepared by dissolving industrial-grade NaCl (99.5 % purity, Fisher Scientific, UK) in distilled water at a concentration of 1.465 g/L.

The draw solution (DS) was prepared using sodium metasilicate (SMS) from Sigma-Aldrich at concentrations of 0.2 M, 0.3 M, 0.4 M, and 0.5 M. Since SMS is highly alkaline, phosphoric acid was used to adjust the pH to 8, ensuring compatibility with the membrane. The resulting reaction products are beneficial to plants, with sodium phosphate providing essential phosphorus for plant growth [29], while silicic acid hydrogel acts as a soil stabilizer [30].

Table 1
Geometrical, physical and chemical specifications of the HFFO module.

HFFO module	Manufacturer	Aquaporin A/S
	Model	HFFO2
	Type	Hollow fiber membrane
	Material	TFC with integrated aquaporin proteins
HFFO Module Dimensions	Module dimensions [b] (mm)	300×70
	Membrane active area [a] (m^2)	2.3
	Active layer charge [a]	Negative
	Fiber Internal Diameter [a] (mm)	0.20
	Fiber Outer Diameter [a] (mm)	0.27
	Fiber length (mm) [b]	270
Recommended Operating Conditions	Operating mode [a]	Counter-current flow
	TMP feed to draw [a] (bar)	0.2
	Temperature Range [a] (°C)	5-30
	pH range	3-10
Operating conditions limits	TMP [a] (bar)	≤ 4
	Feed inlet pressure [a] (bar)	≤ 4
	Draw inlet pressure [a] (bar)	≤ 2
	Free chlorine tolerance [a] (mg/L)	< 0.1
	Temperature [a] (°C)	≤ 50
	pH range	2-11

[a] Value were obtained from the membrane manufacturer
[b] values were obtained from authors

2.3. Experimental setup

A laboratory pilot-plant setup for the FO process was established horizontally, as shown in Fig. 1. The objective was to evaluate FO performance and economic feasibility under various operational conditions. The system consisted of four tanks for FS and DS inlet/outlet. It operated in a batch, single-pass mode using uncirculated FS and DS for each run, allowing straightforward assessment of membrane efficiency.

Operational parameters were monitored using digital balances, pressure meters, flow meters, and conductivity sensors, all connected to an automated data acquisition system logging data every five seconds. The tanks were placed on a digital balance to record weight changes for flow rate and Jw calculations. Flow rates were also measured with F-550 variable area flow meters (Blue-White, USA), and circulation was facilitated by two Masterflex gear pump drives (Cole-Parmer, USA). Conductivity was measured before and after each run using an Orion Star A215 Conductivity Meter (Thermo Fisher Scientific, USA), and TMP was adjusted manually with pressure valves.

Before testing, membranes were flushed with distilled water (1.7 μS/cm) for 45 minutes to stabilize the system. Experiments were conducted in two orientations: FS facing the active layer (AL-FS) and DS facing the active layer (AL-DS). Counter-current flow was selected based on the manufacturer's recommendation and supported by previous studies, which demonstrate its superiority over co-current configurations by enhancing the osmotic pressure gradient across the membrane [31] to [24]. One parameter was varied at a time, while others were held constant, and each test was repeated three times to ensure data reliability. The study tested feed flow rates (40-100 L/h), draw flow rates (25-100 L/h), transmembrane pressure (0-1 bar), and DS molarity (0.2-0.5 M), as detailed in Tables 2 and Table 3.

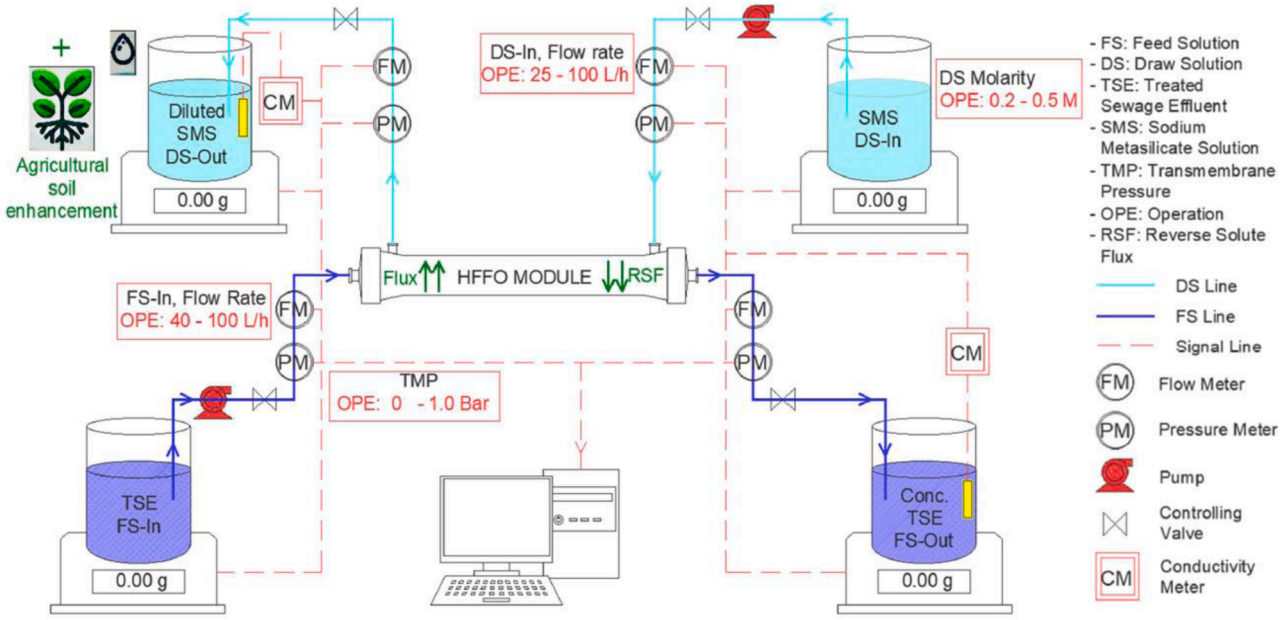

Fig. 1. HFFO experimental setup.

Table 2
Operational parameters of the HFFO performance test.

FS		DS		TMP (bar)	Membrane orientation	Flow direction	Temperature °C
Solution	Flow rate (L/h)	Solution	Flow rate (L/h)				
DI H_2O 1.465 g/L NaCl	40	0.2 M SMS	25	0.3	AL-FS & AL-DS	Counter current	25

Only one of the listed parameters was modified while the others remained constant.

Table 3
Operational parameter modified during the HFFO performance test.

FS flow rate (L/h)	DS flow rate (L/h)	TMP (Bar)	DS Molarity (M)	Membrane Orientation
40	25	0	0.2	AL-F
60	50	0.2	0.3	
80	75	0.3	0.4	AL-D
100	100	1	0.5	

2.4. Performance of forward osmosis

Sensor data (flow rates, conductivity, pressure) were utilized to calculate key performance parameters, including Jw, RSF, SRSF, and water recovery. Also, membrane selectivity was determined using ion chromatography (IC) to measure the rejection of specific ions in the feed and draw solutions.

- - Jw, measured in LMH (L/m²·h), was calculated as:

$$J_w = \frac{Q_{FS,in} - Q_{FS,out}}{A_{Mem}} = \frac{Q_{DS,out} - Q_{DS,in}}{A_{Mem}} \quad (1)$$

where $Q_{FS,in}$, $Q_{FS,out}$, $Q_{DS,in}$ and $Q_{DS,out}$ (L/h) represent the FS and DS flow rates in and out of the membrane, and A_{Mem} is the membrane area.

- RSF measured in GMH ($g.m^{-2}.h^{-1}$), was calculated as:

$$RSF = \frac{\left(\sigma_{FS,out} - \frac{\sigma_{FS,in}}{1-WR}\right) x\ \beta\ x\ Q_{FS,out}}{A_{Mem}} \quad (2)$$

Where $\sigma_{FS,out}$ and $\sigma_{FS,in}$ represent the conductivity of the feed outlet and inlet solution, respectively, and β is the conductivity conversion factor that describes the relation between conductivity and salt concentration. In this paper, β was tested at 0.414 $mg{\cdot}L^{-1}{\cdot}\mu S^{-1}{\cdot}cm$. WR, water recovery, defines the percentage of water in FS passing through the membranes and was calculated as:

$$WR = \frac{Q_{FS,in} - Q_{FS,out}}{Q_{FS,in}}\ x\ 100\% \quad (3)$$

- TMP was determined by the equation:

$$TMP = \frac{P_{FS,in} + P_{FS,out}}{2} - \frac{P_{DS,in} + P_{DS,out}}{2} \quad (4)$$

Where $P_{FS,in}$, $P_{FS,out}$, $P_{DS,in}$ and $P_{DS,out}$ (bar) denote pressure measured at feed inlet, feed outlet, draw inlet and draw outlet, respectively.

- Rejection rate (R) during FO process was calculated as:

$$R = 1 - \frac{C_p}{C_{F,in}} x\ 100\% \quad (5)$$

$$C_p = \frac{C_{DS,out}\ x\ Q_{DS,out}}{Q_{DS,out} - Q_{DS,in}} \quad (6)$$

where C_p, $C_{F,in}$ and $C_{DS,out}$ are the concentrations in the permeate water, FS inlet and DS outlet, respectively.

2.5. Economic analysis of forward osmosis

The techno-economic feasibility of a full-scale FO process was assessed based on laboratory-scale experimental results, including both capital costs and operational costs. Capital costs cover direct expenses such as FS intake, circulation pumps for FS and DS, and FO membrane modules. Site preparation and construction are projected to constitute an additional 10 % of the total equipment expenses. Indirect capital costs, estimated at 27 % of direct costs, cover a range of necessities, including installation services, design fees, and professional expenses [32].

Operational costs include a variety of factors such as, feed intake, circulation pumps, membrane replacement, and membrane operation which is anticipated to be 10 % of the FO membrane's capital cost. Furthermore, operational costs also account for chemical expenses involving the draw and dosing solutions, insurance costs approximated at 0.5 % of the total capital costs, and labor and maintenance expenses estimated at 2 % of the production rate [33,34]. A critical, often underappreciated aspect of operational costs is related to energy consumption for recirculation pumps, representing 25-30 % of total energy demand, which emphasizes the importance of optimizing pump operation reduce energy usage [35].

All calculations for capital costs and operational costs associated with the FO process were adapted from established economic evaluations, using assumptions as detailed in Table 4. Capital costs are in USD and operating costs are in USD per annum.

2.5.1. Capital cost (CC)

- Capital cost of FS intake (CC_{FS_IT}) [33,34]

$$CC_{FS\_IT} = 0.1\ x\ 996(Q_{FS})^{0.8} \quad (7)$$

Where CC_{FS_IT} is the capital cost of FS intake ($), Q_{FS} is the feed flow rate (m^3/day).

Unlike reverse osmosis (RO), forward osmosis does not require pressurization of the FS. This key distinction significantly reduces pretreatment costs, which are estimated to be only 10 % of those associated with conventional RO systems.

Table 4
List of parameters considered in capital cost and operational cost.

Parameter	unit	value	Reference
Plant Production Capacity (Q_{Perm})	m^3/d	100,000	[36,37]
Plant Design Life (DL_P)	years	20	[38–39]
Plant operation time	h/year	8760	[38]
Membrane design life (DL_{Mem})	years	10	[38]
Membrane unit Cost (UC_{Mem})	$/$m^2$	30	[38,33]
Feed Pressure Drop (P_{FS})	bar	2	[38,39]
Draw Pressure Drop (P_{DS})	bar	1	[38]
Pump efficiency (η)	%	0.85	[38,37]
Energy Rate (ER)	$/kWh	0.10	[36,37]
Interest Rate (ir)	%	6	[38,37]
Plant load factor (PL_f)	-	0.9	[38]

- Capital cost of circulation Pumps (CC_{Pumps})

Cost and performance data for pumps from Torishima Pump Company, Japan, known for their corrosion-resistant, multi-stage centrifugal pumps, were incorporated in this study. A power law cost model was employed to establish cost functions for high-pressure pumps, addressing the challenge that pump costs do not straightforwardly correlate with flow rate and pressure. The regression analysis of this data yielded the following approximate cost function for pumps operating at flow rates below 200 m^3/h:

$$CC_{Pumps} = 52\ x\ Q_p\ x\ P_p\ if\ Q_p < 200\ m^3/h \quad (8)$$

Where CC_{Pumps} represents the capital cost of the circulation pumps ($), Q_p is the pump's flow rate (m^3/h) and $\boldsymbol{P_p}$ is the pump's applied pressure (bar). This equation is utilized for both FS and DS [38,34].

- Capital cost of membrane (CC_{Mem})

$$CC_{Mem.} = A_{Mem.}\ x\ UC_{Mem.} \quad (9)$$

Where $CC_{Mem.}$ is the capital cost of the FO membrane ($), $\boldsymbol{A_{Mem.}}$ is the membrane area (m^2) and $\boldsymbol{UC_{Mem.}}$ is the cost per square meter of membrane ($/$m^2$). It is important to note that the lower packing density in FO modules generally results in higher costs compared to RO modules [38,34].

- Capital cost of site development (CC_{site}) [32]

$$CC_{site} = \left(CC_{FS_{IT}} + CC_{Pumps} + CC_{Mem.}\right)\ x\ 0.1 \quad (10)$$

- Direct capital cost (DCC) [38,36,39]

$$\mathrm{DCC} = \left(CC_{FS_{IT}} + CC_{Pumps} + CC_{Mem.} + CC_{site}\right) \quad (11)$$

- Indirect capital cost (ICC) [32]

$$\mathrm{ICC} = DCC\ x\ 0.27 \quad (12)$$

- Total capital cost (TCC) [38,36,39]

$$\mathrm{TCC} = DCC + ICC \quad (13)$$

- Total annualized capital Cost (TACC)

Total Annualized Capital Cost (TACC) is determined using the amortization factor, which is calculated as follows:

$$\mathrm{a} = \frac{ir\ (ir+1)^{DL_P}}{(ir+1)^{DL_P} - 1} \quad (14)$$

$$\mathrm{TACC} = a\ x\ TCC \quad (15)$$

Where a is the amortization factor, *ir* is the interest rate, PDL is the plant design life (years), TCC is the total capital cost ($) and TACC is the total annualized capital cost ($/year) [38,36,39].

2.5.2. Operational cost (OC)

- Operational cost of FS intake (OC_{FS_IT}) [38,36]

$$OC_{FS\_IT} = \frac{0.028\ x\ P_{IT}\ x\ Q_{FS}\ x\ ER}{\eta}\ x\ 365\ x\ PL_f \quad (16)$$

- Operational cost of energy required by pumps (OC_E)

The specific energy consumption (SEC) of the FO process (kWh/m^3) is calculated using Eq. (17) [38,40].

$$SEC = \frac{(P_{FS}\ Q_{FS}) + (P_{DS}\ Q_{DS}) + (TMP\ Q_{FS})}{36\ \eta\ Q_{Perm}} \quad (17)$$

$$OC_E = SEC\ x\ Q_{perm}\ x\ ER\ x\ 365\ x\ PL_f \quad (18)$$

[38,33,34]

- Operational cost of membrane replacement ($OC_{Mem-Rep}$) [38,39]

$$OC_{Mem-Rep} = \frac{CC_{Mem}\ x\ ir}{1-(1+ir)^{-DL_{Mem}}} \quad (19)$$

Eq. (19) calculates the membrane replacement cost in $/year per replaced membrane during its design life. To determine the annual operational cost of membrane replacement over the plant's design life, the result is multiplied by $\frac{DL_{Mem}\ x\ N_{Mem-Rep}}{DL_P}$, where $N_{Mem-Rep}$ is the number of replaced membranes during the plant's design life.

- Operational cost of membrane operation ($OC_{Mem-Ope}$) [33]

$$OC_{Mem-Ope} = 0.1\ x\ CC_{Mem} \quad (20)$$

- Operational cost of chemicals (OC_{Chem}) [33,34]

$$OC_{Chem} = 0.0225\ x\ F_s\ x\ 365\ x\ PL_f \quad (21)$$

Where F_s is total flow rate of the system (m^3/day).

- Operational cost of insurance (OC_i) [33,34]

$$OC_i = 0.005\ x\ TCC \quad (22)$$

- Operational cost of labor and maintenance (OC_i) [33,34]

$$OC_{L\&M} = 0.2\ x\ Q_{Perm}\ x\ 365\ x\ PL_f \quad (23)$$

- Total annualized operational cost (TAOC) [33,34]

$$OC_{L\&M} = OC_{FS\_IT} + OC_E + OC_{Mem-Rep} + OC_{Mem-Ope} + OC_{Chem} + OC_i + OC_{L\&M} \quad (24)$$

- Specific Solution Cost (SSC) [33,34,38]

$$SSC = \frac{\text{TACC} + \text{TAOC}}{Q_{Perm}\ x\ PL_f\ x\ 365} \quad (25)$$

Where SSC is the specific solution cost ($/m^3)

3. Results and discussion

3.1. Performance of forward osmosis

Concentration polarization is divided into internal and external types, with both dilutive and concentrative effects, as shown in Fig. 2. ICP occurs within the membrane's support layer, while ECP takes place at the membrane-solution interface. In AL-FS mode, water permeates from the FS to the DS, leading to dilutive ICP in the support layer, which reduces the osmotic pressure of the DS. Simultaneously, concentrative ECP increases the osmotic pressure of the FS. In AL-DS mode, ICP on the FS side becomes concentrative, raising its osmotic pressure. Meanwhile, dilutive ECP on the DS side lowers the osmotic pressure of the DS.

3.1.1. Effect of FS flow rate

Jw: Feed flow optimization was necessary, as excessively high flow could reduce water recovery, increase reject volumes, and raise energy consumption. concentrative ECP in AL-FS mode and ICP in AL-DS mode could become significant, reducing the osmotic pressure difference and lowering Jw. Therefore, optimizing the feed flow rate was critical to the FO system's performance. The relationship between feed flow rate and Jw for both AL-FS and AL-DS modes is shown in Fig. 3 For AL-FS mode, Jw increased from 7.43 LMH at 40 L/h to 8.63 LMH at 100 L/h, representing a total rise of 16.06 %. Notably, this increase was nonlinear, with 9.36 % total rise occurring just from the first increment, as the flux rose to 8.13 LMH when the flow rate increased from 40 L/h to 60 L/h. Similarly, in AL-DS mode, Jw increased from 11.2 LMH to 12.61 LMH, a total rise of 12.59 %, with the same nonlinear behavior observed. These findings align with those of Al-Musawy et al. [31], Jalab et al. [41], and Sanahuja-Embuena et al. [17], who also observed higher Jw with increased feed flow rates, due to reduced ECP effects. Shibuya et al. [23] similarly noted that flux increased with feed flow rates up to a point, after which it plateaus. Conversely, Akhtar et al. [42] reported minimal impact of feed flow rate on Jw compared to DS flow rate. Li et al. [24] found that feed flow did not significantly affect the osmotic process when using deionized water, suggesting that feed composition must be considered alongside flow rate for optimal FO performance.

RSF: Our experimental results, as shown in Fig. 3 indicated a direct correlation between feed flow rate and RSF. Lower volumetric flow rates of the FS resulted in reduced solute transfer from the DS to the FS, with the lowest RSF observed at 2.74 GMH at a feed flow rate of 40 L/h. In contrast, at a feed flow rate of 100 L/h, the highest reverse diffusion of DS solutes into the feed was recorded, with an RSF of 3.00 GMH of SMS, marking an overall increase of 9.32 % in AL-FS mode and 7.62 % in AL-DS mode compared to the lowest flow rate. Similarly, studies by Al-Musawy et al. [31] and Jalab et al. [41] also observed significant increases in RSF with higher feed flow rates, reporting increments of 47.4 % and 200 %, respectively. Conversely, in cases where feed flow had no significant influence on Jw, a similar lack of effect was noted on RSF (Akhtar et al. and Li et al. [42,24]). The observed increase in RSF with higher feed flow rates is explained by the direct proportionality between Jw and RSF, influenced by the membrane's selectivity. This relationship is driven by intensified convective transport at elevated Jw, which promotes the migration of solutes from the draw solution to the feed side. Similar findings were reported by Jalab et al. [41] and Heo et al. [43], who observed higher RSF with increasing Jw.

SRSF: With increased feed flow rates, Jw rise outpaced that of the RSF, leading to reduced SRSF values from 0.369 g/L to 0.347 g/L in AL-FS mode, and from 0.522 to 0.499 g/L in AL-DS mode as shown in Fig. 3 Contrasting with studies employing NaCl as the DS, in which the SRSF escalated with increased flow rates due to a higher rise in RSF relative to Jw, as reported by Al-Musawy et al. [31] and Jalab et al. [41], our findings highlight the benefits of using sodium metasilicate as a DS attributed to its lower RSF.

3.1.2. Effect of DS flow rate

Theoretically, DS flow rate significantly influences concentration polarization within the membrane. In AL-FS mode, higher DS flow reduces ICP, while in AL-DS mode, it mitigates ECP. Increasing the DS flow reduces its retention time in the FO module, which helps maintain the osmotic driving force and improves both Jw and recovery. However,

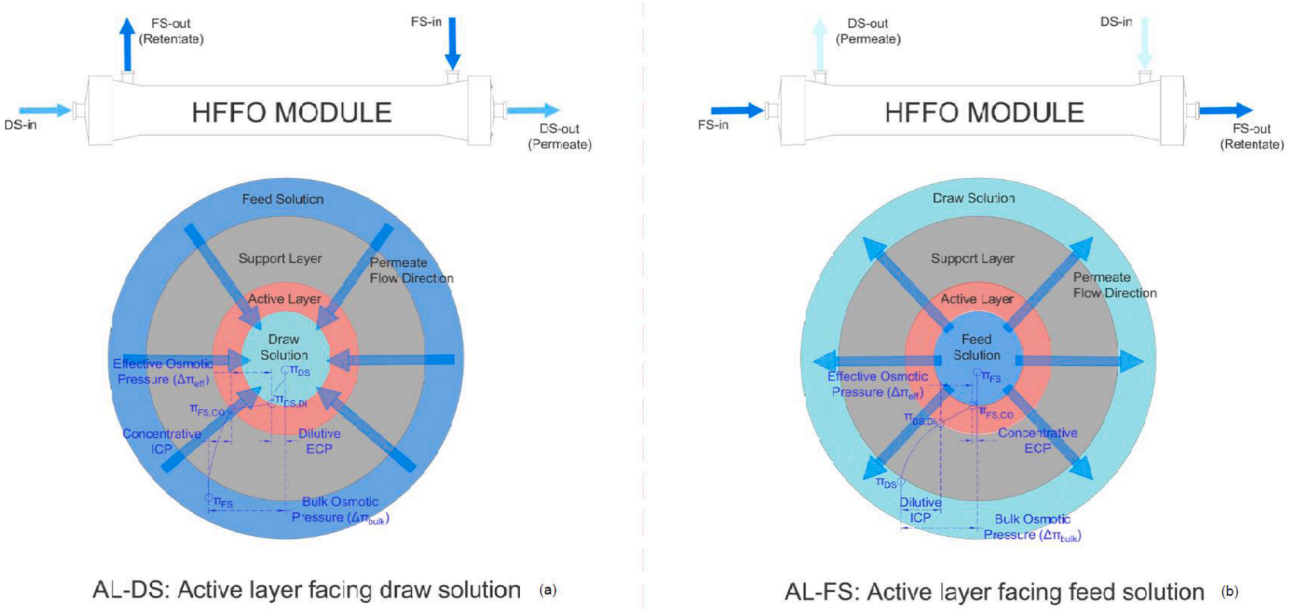

Fig. 2. Impact of concentration polarization on the effective osmotic pressure gradient between draw solution (DS) and feed solution (FS): (a) AL-DS, the osmotic pressure of the draw solution (π_{DS}) decreases due to dilutive external concentration polarization (ECP), yielding ($\pi_{DS,DI}$), while the osmotic pressure of the feed solution (π_{FS}) increases due to concentrative internal concentration polarization (ICP), resulting in ($\pi_{FS,CO}$). (b) AL-FS, π_{DS} decreases due to dilutive ICP, resulting in $\pi_{DS,DI}$, while π_{FS} increases due to concentrative ECP, leading to $\pi_{FS,CO}$.

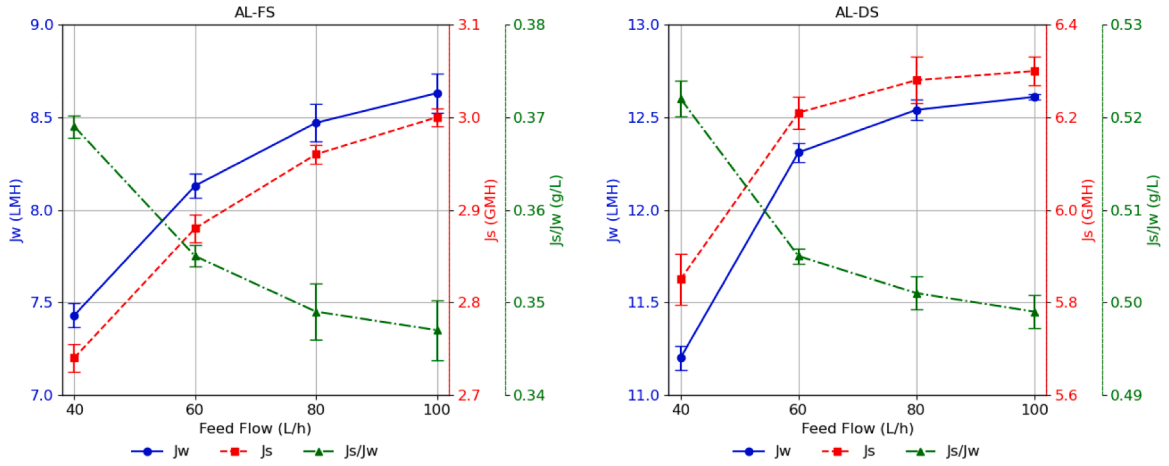

Fig. 3. Effect of FS flow rate on FO performance.

excessively high flow rates can increase energy costs and risk mechanical damage to the hollow fibers, as noted by Sanahuja-Embuena et al. [17].

Jw: Fig. 4 shows that increasing DS flow rates resulted in higher Jw. In AL-FS mode, the membrane demonstrated Jw values of 7.43, 9.51, 10.38, and 10.41 LMH at DS flow rates of 25, 50, 75, and 100 L/h, respectively, translating into a 40.05 % enhancement in flux for a 300 % increase in DS flow rate. Similarly, in AL-DS mode, Jw values increased from 11.2 LMH to 14.26 LMH, marking a 27.34 % rise. The effect of DS flow rate on Jw was more critical in AL-FS mode due to the stronger influence of dilutive ICP compared to ECP. The increase in Jw was nonlinear, plateauing as DS flow rates reached higher levels. This occurs because the maximum concentration achievable in the FO module is the initial DS concentration, which is approached at higher flow rates. Consequently, there is an optimal DS flow rate, beyond which further increase becomes impractical and uneconomical. Our findings are in concordance with the outcomes from a suite of HFFO studies, including those by Jalab et al. [22], Sanahuja-Embuena et al. [44], Akhtar et al., [42], Jalab et al., [41], Sanahuja-Embuena et al., [17] and Shibuya et al., [23] showing a noticeable increase in Jw ranging approximately from 24 % to 34 %. In contrast, Li et al., [24] reported no significant changes in Jw with DS flow, suggesting that the minimum DS rate examined was sufficiently high to mitigate the dilution effect of the DS.

RSF: Fig. 4 shows that increasing DS flow rates intensified solute back diffusion to the feed side. RSF rose from 2.74 GMH to 3.90 GMH in AL-FS mode, and from 5.85 GMH to 8.14 GMH in AL-DS mode. A lower RSF at the minimal DS flow rate studied is desirable, as it minimally reduces the driving force and obviates the need for DS re-concentration. The straightforward relation of RSF and Jw is also confirmed in these experiments. Furthermore, it is noteworthy that the same studies exploring the effects of FS flow rate on Jw also examined the impact of DS flow rate on RSF, consistently revealing an increase in RSF with higher DS flow rates.

SRSF: As shown in Fig. 4, increasing the DS flow rate marginally elevated the draw solute loss per water pass in AL-DS, from 0.522 g/L to 0.571 g/L. However, the DS flow rate's impact on SRSF in AL-FS mode

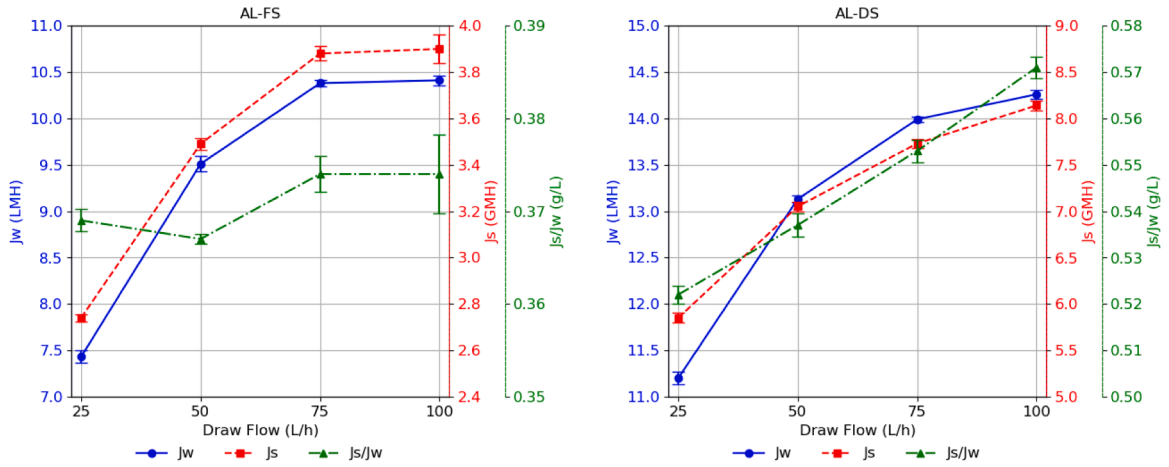

Fig. 4. Effect of DS flow rate on FO performance.

was negligible, as the increase in RSF was offset by a proportional increase in Jw, with SRSF ranging from 0.367 to 0.374 g/L.

The impact of DS flow rate on SRSF reveals a varied landscape among the studies considered. Notably, only a subset of the research previously mentioned has focused on examining changes in SRSF in response to DS flow rate adjustments. Among these, the study conducted by Jalab et al. [22], reported significant rise in SRSF from 1.29 to 2.68 mmol/L as the DS flow rate increased. On the other hand, Sanahuja-Embuena et al. [17] presents a contrasting perspective, suggesting that SRSF remains largely unaffected by variations in DS flow rate.

3.1.3. *Effect of TMP*

FO operates based on the osmotic pressure gradient between the DS and FS, so applied hydraulic pressure typically has a minimal effect on performance since it is well below the osmotic pressure differential.

Jw: As illustrated in Fig. 5, Jw increased slightly from 7.25 to 7.63 LMH in AL-FS mode and from 10.80 to 11.72 LMH in AL-DS mode. This marginal increase is attributed to the additional pressure in the FS, which enhances water transport toward the draw side.

RSF: Fig. 5 showed a slight decrease in RSF was observed as TMP was increased in both membrane orientations. This reduction is rationalized by the requirement for reverse salt diffusion to counteract the added hydraulic pressure from the draw to the feed side, thereby diminishing RSF as TMP increases.

SRSF: As shown in Fig. 5, SRSF decreased as TMP increased, from 0.38 to 0.35 g/L in AL-FS mode and from 0.55 to 0.48 g/L in AL-DS mode.

These results are consistent with those reported by Sanahuja-Embuena et al. [44], Sanahuja-Embuena et al. [17], and Li et al. [24], where only minimal variations in Jw, RSF, and SRSF were noted at elevated TMP. However, FO membrane design, favoring thinner and more fragile supports, limits the extent to which TMP can be increased without risking structural damage.

3.1.4. *Effect of DS concentration*

In theory, an increase in DS concentration is anticipated to enhance the osmotic driving force, thereby elevating Jw across the membrane as well as the RSF.

Jw: As depicted in Fig. 6, Jw increased notably with higher SMS concentrations due to the corresponding rise in osmotic pressure. In AL-FS mode, flux increased from 7.43 LMH at 0.2 M to 12.93 LMH at 0.5 M, with incremental rises at each 0.1 M step (10.72 LMH at 0.3 M and 12.35 LMH at 0.4 M).. Similarly, in AL-DS mode, flux values raised from 11.2 LMH to 17.82 LMH. The flux increase can follow either a linear or asymptotic trend based on DS concentration. Initially, the increase in Jw is linear, where osmotic pressure directly correlates with flux. However, beyond 0.3 M, the rate of flux increase becomes asymptotic due to intensified dilutive concentration polarization, reducing the effectiveness of the DS driving force.

RSF: As shown in Fig. 6, RSF increased significantly with rising SMS concentration, from 2.74 GMH to 7.34 GMH in AL-FS mode, and from 5.85 GMH to 15.82 GMH in AL-DS mode. At 0.5 M, RSF was roughly three times higher than at 0.2 M, indicating that while increasing DS concentration enhances Jw, it disproportionately escalates solute back

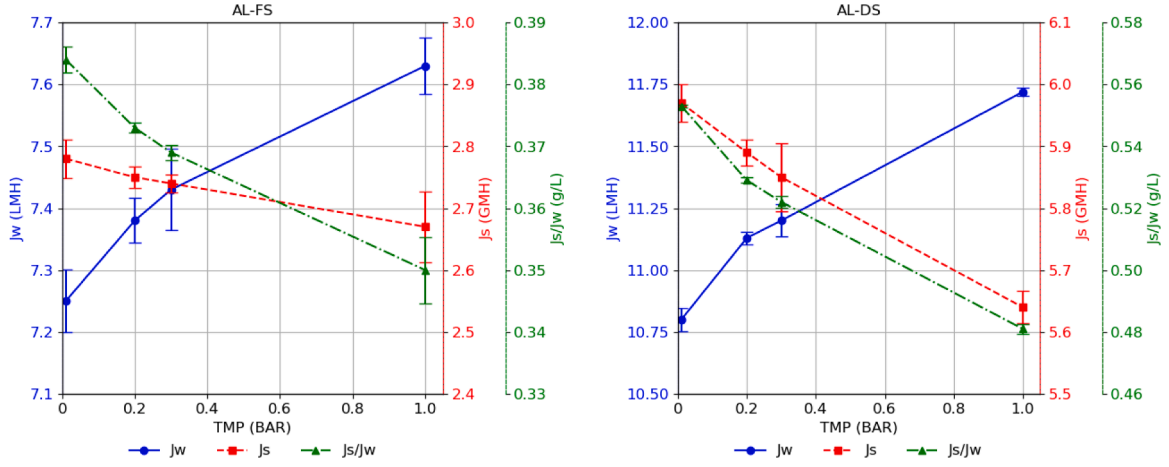

Fig. 5. Effect of TMP on FO performance.

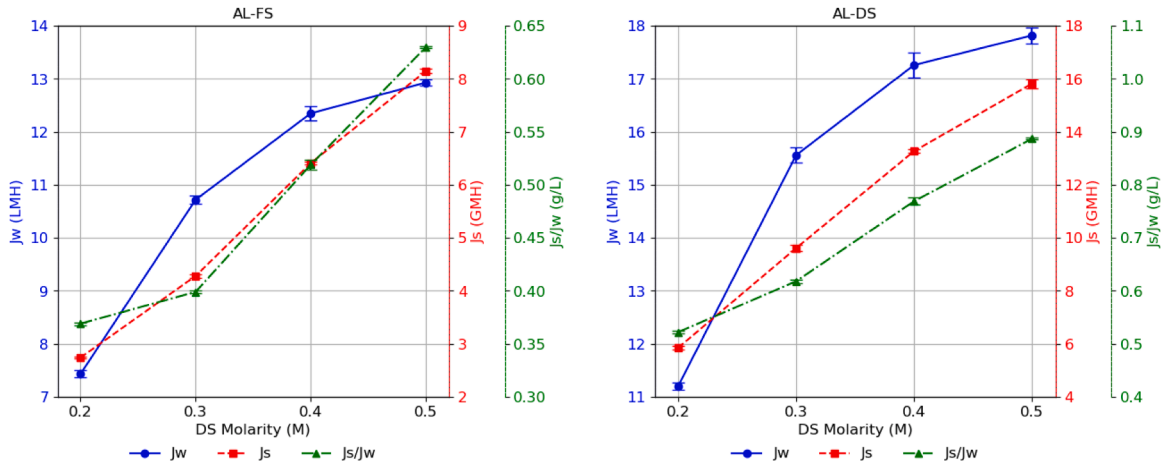

Fig. 6. Effect of DS Molarity on FO performance.

diffusion.

SRSF: As illustrated in Fig. 6, SRSF increased slightly from 0.369 g/L at 0.2 M to 0.399 g/L at 0.3 M in AL-FS mode. At higher concentrations, progressive increase in SRSF was noted, reaching a peak of 0.630 g/L at 0.5 M. A similar trend was observed in AL-DS mode, with SRSF ranging from 0.522 g/L to 0.887 g/L. AL-DS mode showed SRSF values approximately 40 % to 50 % higher than those in AL-FS mode.

The correlation of DS concentration with Jw, RSF, and SRSF aligns with findings reported by Tran et al. [6], and Saiful et al. [45]. Comparable trends have also been observed on HFFO studies by Salih and Al-Alawy [46,47], Salamanca et al. [18], Sanahuja-Embuena et al. [44,17], Al-Musawy W.K. et al. [31], Behboudi et al. [48], Akhtar et al. [42], and Shibuya et al. [23].

3.1.5. Membrane selectivity

The ionic composition of the TSE and diluted DS after the FO process was analyzed using ion chromatography (IC) with a Metrohm IC 850 Pro, as summarized in Table 5. Ion permeation from the TSE into the DS was minimal, with high rejection rates ranging from 87.58 % to 97.81 %, confirming the strong selectivity of the membrane. These results are consistent with those reported by Saiful et al. [45], who also observed high solute rejection using FO membranes.

3.2. Economic analysis of forward osmosis

The influence of FO performance and operational parameters on both CC and OC is summarized in Table 6. Cost increases due to operational adjustments can be offset by improvements in Jw, thereby enhancing overall cost efficiency. When cost savings from increased Jw exceed the additional expenses from operational changes, the system achieves optimal economic performance. However, it is important to note that the findings do not account for the economic associated with RSF.

Table 5
Ionic composition of TSE and diluted DS compared to FAO irrigation limits with removal efficiency (%).

Ions	Concentration (mg/L)				Removal %	
	TSE	Diluted DS		Irrigation Limit		
		AL-FS	AL-DS	FAO [49]	AL-FS	AL-DS
Chloride (Cl)	419.34	20.39	23.02	142.0	95.14	94.51
Nitrate (NO3)	22.33	1.48	1.74	5.0	93.36	92.21
Sulfate (SO4)	205.79	4.88	6.15	20.0	97.63	97.01
Calcium (Ca)	77.75	3.18	9.65	20.0	95.91	87.58
Magnesium (Mg)	21.41	0.47	0.98	5.0	97.81	95.43

3.2.1. Effect of FS flow rate

Increasing the FS flow rate had a noticeable impact on both capital and operational costs, with the most significant changes observed in $\boldsymbol{CC_{FS\_IT}}$, $\boldsymbol{CC_{Pumps}}$, $\boldsymbol{OC_{FS\_IT}}$ and $\boldsymbol{OC_{Chem}}$. As the FS flow rate increased, related costs escalated by 65 % to 122 % due to higher capacity and power needs for managing larger volumes. However, the rise in costs was non-linear. The non-linear increase in Jw with higher flow rates moderated some cost escalations, particularly for membrane-related expenses, partially offsetting additional costs. Fig. 7(a) shows the annual costs for varying feed flow rates.

3.2.2. Effect of DS flow rate

An increase in the DS flow rate had a significant impact on both capital and operational costs, with the most notable changes occurring in CC_{Pumps}, CC_{Mem}, OC_E, $OC_{Mem-Rep}$, $OC_{Mem-Ope}$, and OC_{Chem}. The optimal cost was achieved at 50 L/h, where the increase in flux from 25 L/h to 50 L/h resulted in substantial savings in membrane-related capital and operational costs. Beyond 50 L/h, although flux continued to increase, the rate of improvement diminishes, and the resulting operational cost reductions are insufficient to offset the rising capital and operational expenses related to pumps, energy, and DS consumption. Consequently, the system's overall economic efficiency declined at DS flow rates higher than 50 L/h. This trend is clearly illustrated in Fig. 7(b), which outlined the annual breakdown of capital and operational costs across varying DS flow rates.

3.2.3. Effect of TMP

Increasing TMP primarily resulted in a rise in OC_E, as additional energy was required. However, this was fully offset by slight decreases in other capital and operational costs, with overall costs decreasing by up to 5 % in AL-FS mode and 7.8 % in AL-DS mode. These savings were attributed to improved Jw, which reduced the membrane area and associated costs. The overall relationship between TMP and the annual cost distribution is shown in Fig. 7(c).

3.2.4. Effect of DS concentration

As noted under Fig. 7(d), increasing the DS concentration had the highest impact on capital and operational costs. The most significant cost reductions occurred between 0.2 M and 0.3 M, driven by a substantial increase in flux and water recovery, leading to minimized costs across most categories. Between 0.3 M and 0.4 M, costs continued to decrease, but at a slower rate. However, from 0.4 M to 0.5 M, costs began to rise slightly as the flux improvements no longer offset the increasing DS expenses under OC_{Chem}.

Table 6
Influence of FO operational parameters and performance on capital and operational costs.

Cost Impact		FO Performance	FO Operational Parameters (Impacting FO Performance)			
		Jw & Recovery	FS Flow Rate	DS Flow Rate	TMP	Molarity
CC	CC_{FS-IT}	Decrease	Increase	-	-	-
	CC_{Pumps}	Decrease	Increase	Increase	Increase	-
	$CC_{Mem.}$	Decrease	-	-	-	-
	CC_{Site}	Decrease	Increase	Increase	Increase	-
	$CC_{Indirect}$	Decrease	Increase	Increase	Increase	-
OC	OC_{FS-IT}	Decrease	Increase	-	-	-
	OC_{E}	Decrease	Increase	Increase	Increase	-
	OC_{MEM_Rep}	Decrease	-	-	-	-
	OC_{MEM_Ope}	Decrease	-	-	-	-
	OC_{Chem}	Decrease	Increase	Increase	-	Increase
	OCi	Decrease	Increase	Increase	Increase	-
	$OC_{L\&M}$	-	-	-	-	-

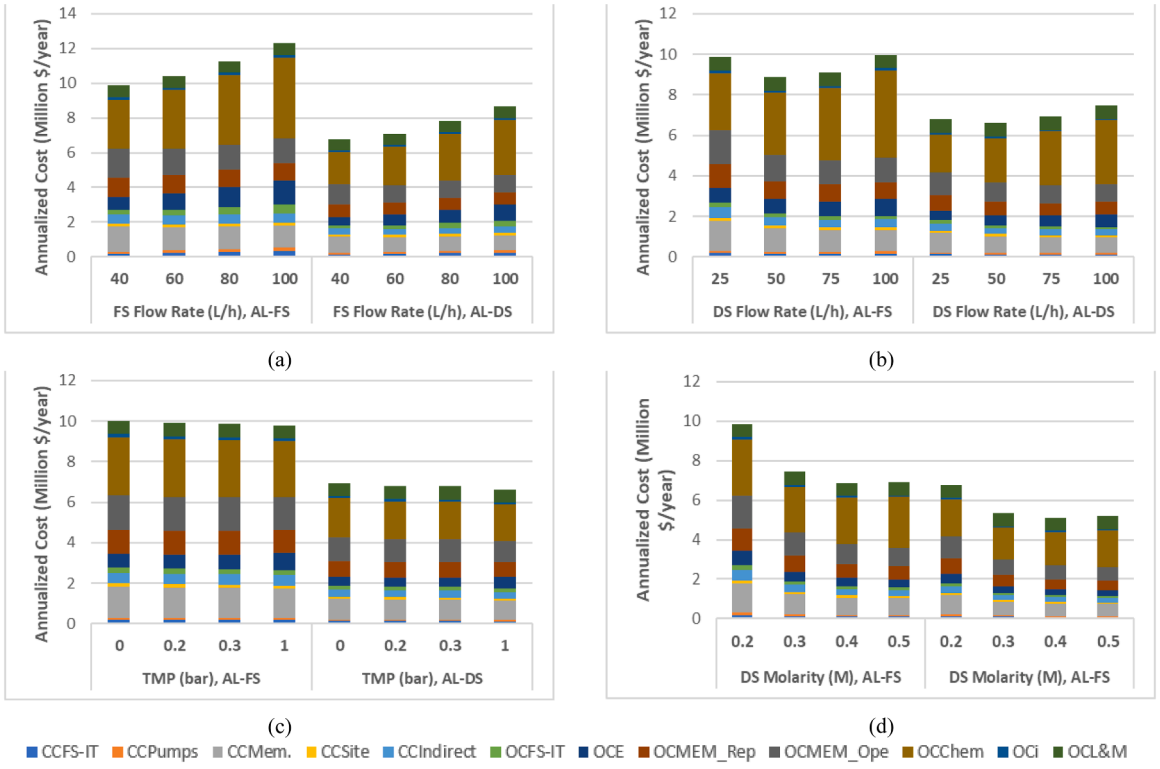

Fig. 7. Annual cost analysis of FO System Under Different Operating Conditions.

3.2.5. *Effect of Membrane orientation*

As illustrated in Fig. 7, AL-DS consistently demonstrated lower overall costs, primarily due to the higher Jw in this configuration. The increased Jw improved water recovery efficiency, reducing both capital and operational expenses, making AL-DS more cost-effective. However, it is important to note that while AL-DS offered cost benefits, it also experienced significantly higher SRSF compared to AL-FS.

3.2.6. *Specific solution cost (SSC)*

The specific solution cost (SSC) for both AL-FS and AL-DS modes was evaluated under varying operational parameters. In AL-FS mode, SSC ranged between 0.21 and 0.37 $/m^3, while in AL-DS mode, SSC was lower, ranging from 0.16 to 0.26 $/m^3. Compared to literature values, Hafiz et al. [38] reported SSC of 0.48 $/m^3, and Choi et al. [36] found water costs in FO-RO hybrid system ranging from 0.71 to 0.84 $/m^3, both significantly higher than our findings. Furthermore, Patel et al. [33] reported SSC of 0.37 $/m^3, while in another study, Patel et al. [34] estimated SSC of 0.23 $/m^3. These results demonstrated that SMS provided considerable economic advantages, especially under optimized operational parameters. The cited studies similarly accounted for both CAPEX and OPEX in their SSC evaluations and were based on comparable baseline assumptions, including plant capacity, design life, membrane cost, and the use of wastewater or brine as feed solution.

4. Conclusion

This study successfully demonstrated the feasibility of using hollow fiber forward osmosis (FO) membranes to effectively dilute sodium metasilicate (SMS)-based sol-gel as a novel DS, offering a sustainable approach to addressing water scarcity. Utilizing TSE as the FS not only facilitated the dilution of the SMS but also effectively addressed wastewater reuse challenges. The findings revealed that optimal feed and DS flow rates of 60–80 L/h and 50–75 L/h, respectively, maximized Jw while minimizing SRSF. Furthermore, increasing SMS molarity

beyond 0.3 M improved Jw; however, it also caused a disproportionate rise in RSF, highlighting the need for a balance between efficiency and solute loss. TMP, optimized within the range of 0.2–0.3 bar, had minimal impact on Jw but effectively mitigated RSF, ensuring improved operational efficiency. Membrane orientation played a significant role in performance, with the active layer facing the DS (AL-DS mode) resulting in higher Jw due to reduced internal concentration polarization; however, it also led to increased RSF compared to the active layer facing the FS (AL-FS mode). Notably, the maximum Jw achieved was 17.82 LMH, while membrane selectivity demonstrated high ion rejection rates of up to 97.8 %. Economic analysis indicated that AL-DS mode offered lower specific solution costs ($0.16–$0.26/m^3) compared to AL-FS mode ($0.21–$0.37/m^3), reinforcing the economic feasibility of the system for large-scale implementation. Among the examined operational parameters, DS concentration had the most significant impact on costs, with major reductions observed when increasing concentration from 0.2 M to 0.3 M due to enhanced Jw and recovery; however, diminishing returns were noted at higher concentrations. Overall, the optimized FO process presents an efficient and cost-effective solution for water-scarce regions, contributing to sustainable water resource management and wastewater reuse initiatives.

CRediT authorship contribution statement

Firas Alkadour: Writing – original draft, Formal analysis, Data curation, Conceptualization. **Kenan A. Alkhamri:** Formal analysis, Data curation. **Tayma Kazwini:** Formal analysis, Data curation. **Ali Altaee:** Writing – review & editing, Methodology, Conceptualization. **Maryam AL-Ejji:** Writing – review & editing, Conceptualization. **Probir Das:** Writing – review & editing, Conceptualization. **Alaa H. Hawari:** Writing – review & editing, Supervision, Methodology, Investigation, Conceptualization.

Declaration of competing interest

The authors declare that they have no known competing financial interests or personal relationships that could have appeared to influence the work reported in this paper.

Acknowledgments

This work was supported by the Qatar National Research Fund [grant number MME03-1015-210003]; and the Graduate Sponsorship Research Award, Qatar National Research Fund [grant number GSRA7-1-0511-20048].

The authors acknowledge the Central Laboratories Unit (CLU) at Qatar University for their assistance with ion chromatography analysis. The content is solely the responsibility of the authors and does not necessarily represent the official views of the funding agencies.

Data availability

Data will be made available on request.

References

[1] Claude H Hurley, Thomas H Thornburn, Sodium silicate stabilization of soils: a review of the literature. Highway research record, Highway Research Board, National Research Council, Washington, 1972 no. no.

[2] H.S. Siam, A.E.-M.M.R.S.A. Mahmoud, G.W. Ageeb, M.G. Abd El Kader, Ameliorative effect of silicate in soil and plant. A review, Curr. Sci. Int. (2022), https://doi.org/10.36632/csi/2022.11.1.3.

[3] G.Z. Qin, S.P. Tian, Enhancement of biocontrol activity of cryptococcus laurentii by Silicon and the possible mechanisms involved, Phytopathology. 95 (1) (2005) 69–75, https://doi.org/10.1094/PHYTO-95-0069. Jan.

[4] M. Mali, N.C. Aery, Influence of silicon on growth, relative water contents and uptake of silicon, calcium and potassium in wheat grown in nutrient solution, J. Plant Nutr. 31 (11) (2008) 1867–1876, https://doi.org/10.1080/01904160802402666. Oct.

[5] X. Zhou, Y. Shen, X. Fu, F. Wu, Application of sodium silicate enhances cucumber resistance to fusarium wilt and alters soil microbial communities, Front. Plant Sci. 9 (2018) 624, https://doi.org/10.3389/fpls.2018.00624. May.

[6] A.T.K. Tran, N.T.T. Hoang, N.D. Dat, Phosphate pre-concentration from wastewater by a continuous flow bench-scale forward osmosis membrane: A circular economy approach on nutrient recovery, Results. Eng. 24 (2024) 103247, https://doi.org/10.1016/j.rineng.2024.103247. Dec.

[7] J.L. Soler-Cabezas, J.A. Mendoza-Roca, M.C. Vincent-Vela, M.J. Luján-Facundo, L. Pastor-Alcañiz, Simultaneous concentration of nutrients from anaerobically digested sludge centrate and pre-treatment of industrial effluents by forward osmosis, Sep. Purif. Technol. 193 (2018) 289–296, https://doi.org/10.1016/j.seppur.2017.10.058. Mar.

[8] B. Honmane, T. Deshpande, A. Dhand, R. Bhansali, P.K. Ghosh, Channelizing the osmotic energy of proximate sea bittern for concentration of seawater by forward osmosis under realistic conditions to conserve land requirement for solar sea salt production, J. Memb. Sci. 567 (2018) 329–338, https://doi.org/10.1016/j.memsci.2018.09.022. Dec.

[9] T. Hey, N. Bajraktari, J. Vogel, C. Hélix Nielsen, J. La Cour Jansen, K. Jönsson, The effects of physicochemical wastewater treatment operations on forward osmosis, Environ. Technol. 38 (17) (2017) 2130–2142, https://doi.org/10.1080/09593330.2016.1246616. Sep.

[10] T. Yoshioka, et al., Molecular dynamics simulation study of polyamide membrane structures and RO/FO water permeation properties, Membranes. (Basel) 8 (4) (2018) 127, https://doi.org/10.3390/membranes8040127. Dec.

[11] F.M. Munshi, et al., Dewatering algae using an aquaporin-based polyethersulfone forward osmosis membrane, Sep. Purif. Technol. 204 (2018) 154–161, https://doi.org/10.1016/j.seppur.2018.04.077. Oct.

[12] W. Xu, Q. Chen, Q. Ge, Recent advances in forward osmosis (FO) membrane: chemical modifications on membranes for FO processes, Desalination. 419 (2017) 101–116, https://doi.org/10.1016/j.desal.2017.06.007. Oct.

[13] J.M. Tharayil, P. Chinnaiyan, D.M. John, K. M S, Environmental sustainability of FO membrane separation applications – Bibliometric analysis and state-of-the-art review, Results. Eng. 21 (2024) 101677, https://doi.org/10.1016/j.rineng.2023.101677. Mar.

[14] G. Junco, V. Migo, M.M. Magboo, R.C. Eusebio, Selection of optimal draw solution recovery technology for forward osmosis desalination system using analytical hierarchy process, PalawanSci 16 (1) (2024) 38–47, https://doi.org/10.69721/TPS.J.2024.16.1.05. Jun.

[15] T. Kazwini, et al., Sodium metasilicate sol-gel draw solution for seawater desalination and supplementing nutrients to soil, Desalination. 600 (2025) 118517, https://doi.org/10.1016/j.desal.2024.118517. May.

[16] Y. Wibisono, V. Noviani, A.T. Ramadhani, L.A. Devianto, A.A. Sulianto, Eco-friendly forward osmosis membrane manufacturing using dihydrolevoglucosenone, Results. Eng. 16 (2022) 100712, https://doi.org/10.1016/j.rineng.2022.100712. Dec.

[17] V. Sanahuja-Embuena, et al., Role of operating conditions in a pilot scale investigation of hollow Fiber forward osmosis membrane modules, Membranes. (Basel) 9 (6) (2019) 66, https://doi.org/10.3390/membranes9060066. Jun.

[18] M. Salamanca, R. López-Serna, L. Palacio, A. Hernandez, P. Prádanos, M. Peña, Ecological risk evaluation and removal of emerging pollutants in urban wastewater by a hollow Fiber forward osmosis membrane, Membranes. (Basel) 12 (3) (2022) 293, https://doi.org/10.3390/membranes12030293. Mar.

[19] P.S. Goh, A.F. Ismail, B.C. Ng, M.S. Abdullah, Recent progresses of forward osmosis membranes formulation and design for wastewater treatment, Water. (Basel) 11 (10) (2019) 2043, https://doi.org/10.3390/w11102043. Sep.

[20] R. Kapilan, M. Vaziri, J.J. Zwiazek, Regulation of aquaporins in plants under stress, Biol. Res. 51 (1) (2018) 4, https://doi.org/10.1186/s40659-018-0152-0. Dec.

[21] Y. Li, Z. Xu, M. Xie, B. Zhang, G. Li, W. Luo, Resource recovery from digested manure centrate: comparison between conventional and aquaporin thin-film composite forward osmosis membranes, J. Memb. Sci. 593 (2020) 117436, https://doi.org/10.1016/j.memsci.2019.117436. Jan.

[22] R. Jalab, et al., Investigation of thin-film composite hollow fiber forward osmosis membrane for osmotic concentration: A pilot-scale study, Korean J. Chem. Eng. 39 (1) (2022) 178–188, https://doi.org/10.1007/s11814-021-0935-9. Jan.

[23] M. Shibuya, M. Yasukawa, T. Takahashi, T. Miyoshi, M. Higa, H. Matsuyama, Effect of operating conditions on osmotic-driven membrane performances of cellulose triacetate forward osmosis hollow fiber membrane, Desalination. 362 (2015) 34–42, https://doi.org/10.1016/j.desal.2015.01.031. Apr.

[24] R. Li, S. Braekevelt, J.L.N. De Carfort, S. Hussain, U.E. Bollmann, K. Bester, Laboratory and pilot evaluation of aquaporin-based forward osmosis membranes for rejection of micropollutants, Water. Res. 194 (2021) 116924, https://doi.org/10.1016/j.watres.2021.116924. Apr.

[25] J.R. Mccutcheon, M. Elimelech, Modeling water flux in forward osmosis: implications for improved membrane design, AIChE J. 53 (7) (2007) 1736–1744, https://doi.org/10.1002/aic.11197. Jul.

[26] J.R. Werber, A. Deshmukh, M. Elimelech, The critical need for increased selectivity, not increased water permeability, for desalination membranes, Environ. Sci. Technol. Lett. 3 (4) (2016) 112–120, https://doi.org/10.1021/acs.estlett.6b00050. Apr.

[27] Y. Chun, D. Mulcahy, L. Zou, I. Kim, A short review of membrane fouling in forward osmosis processes, Membranes. (Basel) 7 (2) (2017) 30, https://doi.org/10.3390/membranes7020030. Jun.

[28] H. Huang, H. Zhang, F. Xiao, J. Liang, Y. Wu, Efficient removal of fluoride ion by the composite forward osmosis membrane with modified cellulose nanocrystal interlayer, Results. Eng. 20 (2023) 101449, https://doi.org/10.1016/j.rineng.2023.101449. Dec.

[29] L.F. Lugli, et al., Rapid responses of root traits and productivity to phosphorus and cation additions in a tropical lowland forest in Amazonia, New Phytologist 230 (1) (2021) 116–128, https://doi.org/10.1111/nph.17154. Apr.
[30] D.N. Kalbuadi, L.P. Santi, D.H. Goenadi, J. Barus, Application of bio-silicic acid to improve yield and fertilizer efficiency of paddy on tidal swamp land, MP 88 (2) (2020), https://doi.org/10.22302/iribb.jur.mp.v88i2.378. Oct.
[31] W. Kh. Al-Musawy, M.H. Al-Furaiji, Q.F. Alsalhy, Synthesis and characterization of PVC-TFC hollow fibers for forward osmosis application, J of Applied Polymer Sci 138 (35) (2021) 50871, https://doi.org/10.1002/app.50871. Sep.
[32] A. Malek, M.N.A. Hawlader, J.C. Ho, Design and economics of RO seawater desalination, Desalination. 105 (3) (1996) 245–261, https://doi.org/10.1016/0011-9164(96)00081-1. Jul.
[33] D. Patel, A. Mudgal, V. Patel, J. Patel, Techno-economic analysis of forward osmosis system for domestic wastewater treatment, Materials Today: Proceedings 77 (2023) 69–74, https://doi.org/10.1016/j.matpr.2022.08.560.
[34] D. Patel, et al., Energy, exergy, economic and environment analysis of standalone forward osmosis (FO) system for domestic wastewater treatment, Desalination. 567 (2023) 116995, https://doi.org/10.1016/j.desal.2023.116995. Dec.
[35] S. Zou, H. Yuan, A. Childress, Z. He, Energy consumption by recirculation: A missing parameter when evaluating forward osmosis, Environ. Sci. Technol. 50 (13) (2016) 6827–6829, https://doi.org/10.1021/acs.est.6b02849. Jul.
[36] Y. Choi, H. Cho, Y. Shin, Y. Jang, S. Lee, Economic evaluation of a hybrid desalination system combining forward and reverse osmosis, Membranes. (Basel) 6 (1) (2015) 3, https://doi.org/10.3390/membranes6010003. Dec.
[37] S.J. Im, S. Jeong, S. Jeong, A. Jang, Techno-economic evaluation of an element-scale forward osmosis-reverse osmosis hybrid process for seawater desalination, Desalination. 476 (2020) 114240, https://doi.org/10.1016/j.desal.2019.114240. Feb.
[38] M. Hafiz, R. Alfahel, A. Altaee, A.H. Hawari, Techno-economic assessment of forward osmosis as a pretreatment process for mitigation of scaling in multi-stage flash seawater desalination process, Sep. Purif. Technol. 309 (2023) 123007, https://doi.org/10.1016/j.seppur.2022.123007. Mar.
[39] A. Zarebska-Mølgaard, et al., Techno-economic assessment of a hybrid forward osmosis and membrane distillation system for agricultural water recovery, Sep. Purif. Technol. 283 (2022) 120196, https://doi.org/10.1016/j.seppur.2021.120196. Jan.
[40] M. Hafiz, R. Alfahel, A.H. Hawari, M.K. Hassan, A. Altaee, A hybrid NF-FO-RO process for the supply of irrigation water from treated wastewater: simulation study, Membranes. (Basel) 11 (3) (2021) 191, https://doi.org/10.3390/membranes11030191. Mar.
[41] R. Jalab, A.M. Awad, M.S. Nasser, J. Minier-Matar, S. Adham, Pilot-scale investigation of flowrate and temperature influence on the performance of hollow fiber forward osmosis membrane in osmotic concentration process, J. Environ. Chem. Eng. 8 (6) (2020) 104494, https://doi.org/10.1016/j.jece.2020.104494. Dec.
[42] A. Akhtar, M. Singh, S. Subbiah, K. Mohanty, Sugarcane juice concentration using a novel aquaporin hollow fiber forward osmosis membrane, Food and Bioproducts Processing 126 (2021) 195–206, https://doi.org/10.1016/j.fbp.2021.01.007. Mar.
[43] J. Heo, et al., Organic fouling and reverse solute selectivity in forward osmosis: role of working temperature and inorganic draw solutions, Desalination. 389 (2016) 162–170, https://doi.org/10.1016/j.desal.2015.06.012. Jul.
[44] V. Sanahuja-Embuena, J. Frauholz, T. Oruc, K. Trzaskus, C. Hélix-Nielsen, Transport mechanisms behind enhanced solute rejection in forward osmosis compared to reverse osmosis mode, J. Memb. Sci. 636 (2021) 119561, https://doi.org/10.1016/j.memsci.2021.119561. Oct.
[45] S.Hasima Saiful, N. Kamila, Rahmi, Cellulose acetate from palm oil bunch waste for forward osmosis membrane in desalination of brackish water, Results. Eng. 15 (2022) 100611, https://doi.org/10.1016/j.rineng.2022.100611. Sep.
[46] M.H. Salih, A.F. Al-Alawy, MgCl2 and MgSO4 as draw agents in forward osmosis process for east Baghdad oilfield produced water treatment, DWT 256 (2022) 80–88, https://doi.org/10.5004/dwt.2022.28408.
[47] M.H. Salih, A.F. Al-Alawy, A novel forward osmosis for treatment of high-salinity East Baghdad oilfield produced water as a part of a zero liquid discharge system, DWT 248 (2022) 18–27, https://doi.org/10.5004/dwt.2022.28070.
[48] A. Behboudi, S. Ghiasi, T. Mohammadi, M. Ulbricht, Preparation and characterization of asymmetric hollow fiber polyvinyl chloride (PVC) membrane for forward osmosis application, Sep. Purif. Technol. 270 (2021) 118801, https://doi.org/10.1016/j.seppur.2021.118801. Sep.
[49] R. S. Ayers and D. W. Westcot, Water quality for agriculture. in FAO irrigation and drainage paper, no. 29, rev. 1. Rome: Food and Agriculture Organization of the United Nations, 1985.